nature genetics

Disruption of the basal body compromises proteasomal function and perturbs intracellular Wnt response

Jantje M Gerdes[1], Yangfan Liu[1], Norann A Zaghloul[1], Carmen C Leitch[1], Shaneka S Lawson[1], Masaki Kato[2,6], Philip A Beachy[2,6], Philip L Beales[3], George N DeMartino[4], Shannon Fisher[1], Jose L Badano[1,5] & Nicholas Katsanis[1,6,7]

Primary cilia and basal bodies are evolutionarily conserved organelles that mediate communication between the intracellular and extracellular environments. Here we show that *bbs1*, *bbs4* and *mkks* (also known as *bbs6*), which encode basal body proteins, are required for convergence and extension in zebrafish and interact with *wnt11* and *wnt5b*. Suppression of *bbs1*, *bbs4* and *mkks* transcripts results in stabilization of β-catenin with concomitant upregulation of T-cell factor (TCF)-dependent transcription in both zebrafish embryos and mammalian ciliated cells, a defect phenocopied by the silencing of the axonemal kinesin subunit *KIF3A* but not by chemical disruption of the cytoplasmic microtubule network. These observations are attributable partly to defective degradation by the proteasome; suppression of *BBS4* leads to perturbed proteasomal targeting and concomitant accumulation of cytoplasmic β-catenin. Cumulatively, our data indicate that the basal body is an important regulator of Wnt signal interpretation through selective proteolysis and suggest that defects in this system may contribute to phenotypes pathognomonic of human ciliopathies.

Secreted Wnt proteins propagate an array of cellular responses that influence the fate and function of both embryonic and adult tissues[1]. After Wnt proteins bind to receptors of the Frizzled (Fz) family, the Wnt signal is transmitted to the primarily cytoplasmic protein Disheveled (Dvl), which determines which Wnt signaling pathway will be activated and acts as a switch between canonical and non-canonical Wnt signaling[2]. The canonical, and most extensively characterized, pathway is the β-catenin Wnt pathway. In unstimulated cells, β-catenin is phosphorylated by a complex of axin, adenomatous polyposis coli (APC) and glycogen synthase kinase 3β (GSK3β) and is targeted for proteolytic degradation[3]. Activation of the Wnt pathway results in the destruction of the GSK3β-axin-APC complex, inhibition of GSK3β and stabilization of β-catenin. This results in the elevation of β-catenin cytoplasmic and nuclear levels, coupled with increased levels of nuclear Dvl[3] and subsequent gene expression regulated by β-catenin–TCF-responsive elements, such as axin2 (refs. 4,5). By contrast, in the non-canonical Wnt pathway, Dvl is recruited to the plasma membrane through a mechanism that is not well understood [6,7].

One aspect of non-canonical Wnt signaling is the planar cell polarity (PCP) pathway, which regulates the polarization of cells in the plane of the epithelium. In *Drosophila melanogaster*, a group of 'core' PCP proteins (including the transmembrane proteins frizzled (Fz), van gogh (Vang; also known as strabismus, Stbm) and starry night (Stan), the cytoplasmic signaling components disheveled (Dsh), prickle (Pk) and diego (Dgo) and the cadherin-related proteins fat (Ft) and dachous (Ds)) function in the regulation of wing hair, body bristle and ommatidial polarity[8,9]. Studies in vertebrates have indicated that orthologs of genes encoding PCP proteins have roles in the regulation of polarized cell movements, including defects in convergent extension during gastrulation, when cells move toward the midline and enable anterio-posterior elongation, mediolateral narrowing of the embryo and neural tube closure[8]. In zebrafish, convergent extension defects manifest as mediolaterally elongated somites, broadened notochord, shortened embryonic body axis and reduced intraocular distance; in mice, mutations in the PCP protein–encoding genes *Vangl2*, *Celsr1* and *Scrb1* cause neural tube defects, failure in eyelid closure and disorganization of stereociliary bundles in cochlear sensory hair cells[10–14].

Primary cilia are evolutionarily conserved structures that typically protrude from the apical surface of cells. Initial studies in model organisms linked cilia to chemosensory and mechanosensory roles, and more recent findings have also implicated these organelles in the sensing of morphogenetic signals, most notably those from sonic hedgehog (Shh)[15–17]. Here we present data indicating that the cilium and basal body are involved in regulation of Wnt signaling by a

[1]McKusick-Nathans Institute of Genetic Medicine, Johns Hopkins University School of Medicine, Baltimore, Maryland 21205, USA. [2]Department of Developmental Biology, Institute for Stem Cell Biology and Regenerative Medicine, Howard Hughes Medical Institute, Stanford University School of Medicine, Stanford, California 94305, USA. [3]Molecular Medicine Unit, Institute of Child Health, University College London, WC1N 1EH, UK, [4]Department of Physiology, University of Texas Southwestern Medical Center, Dallas, Texas 75390, USA. [5]Institut Pasteur, CP11400 Montevideo, Uruguay. [6]Department of Molecular Biology and Genetics, [7]Wilmer Eye Institute, Johns Hopkins University School of Medicine, Baltimore, Maryland 21205, USA. Correspondence should be addressed to N.K. (katsanis@jhmi.edu).

Received 20 July; accepted 16 August; published online 30 September 2007; doi:10.1038/ng.2007.12

combination of selective proteolysis and regulation of phosphorylation and that defective Wnt signaling may be causally related to a number of phenotypes associated with ciliopathies.

RESULTS

Bbs1, Bbs4 and Mkks are needed for convergent extension

We have previously shown that suppression of *bbs4* enhances convergent extension defects of the zebrafish mutation *trilobite* (orthologous to *Vangl2*; ref.18), and that suppression of *bbs1, bbs4* and *mkks* phenocopies somitic and notochordal defects of PCP mutants[19]. To investigate whether Bbs1, Bbs4 and Mkks are necessary for convergent extension, we examined embryos depleted of these proteins for disturbances in convergent extension movements. We designed antisense translation-blocking morpholinos against the unique zebrafish orthologs of *bbs1*, *bbs4* and *mkks* and injected them into wild-type (WT) embryos. Scoring of >100 embryos by two investigators blinded to the experiment showed that each morpholino injection produced dose-dependent features characteristic of convergent extension defects (**Fig. 1**), such as shortened body axes and longer somites, as judged by staining with riboprobes against *myoD*, *krox20* and *pax2* (**Fig. 1a**,**b**,**e–h**). Moreover, we observed aberrant posterior *myoD* staining (**Fig. 1f–h**) that coincided with tail extension defects in

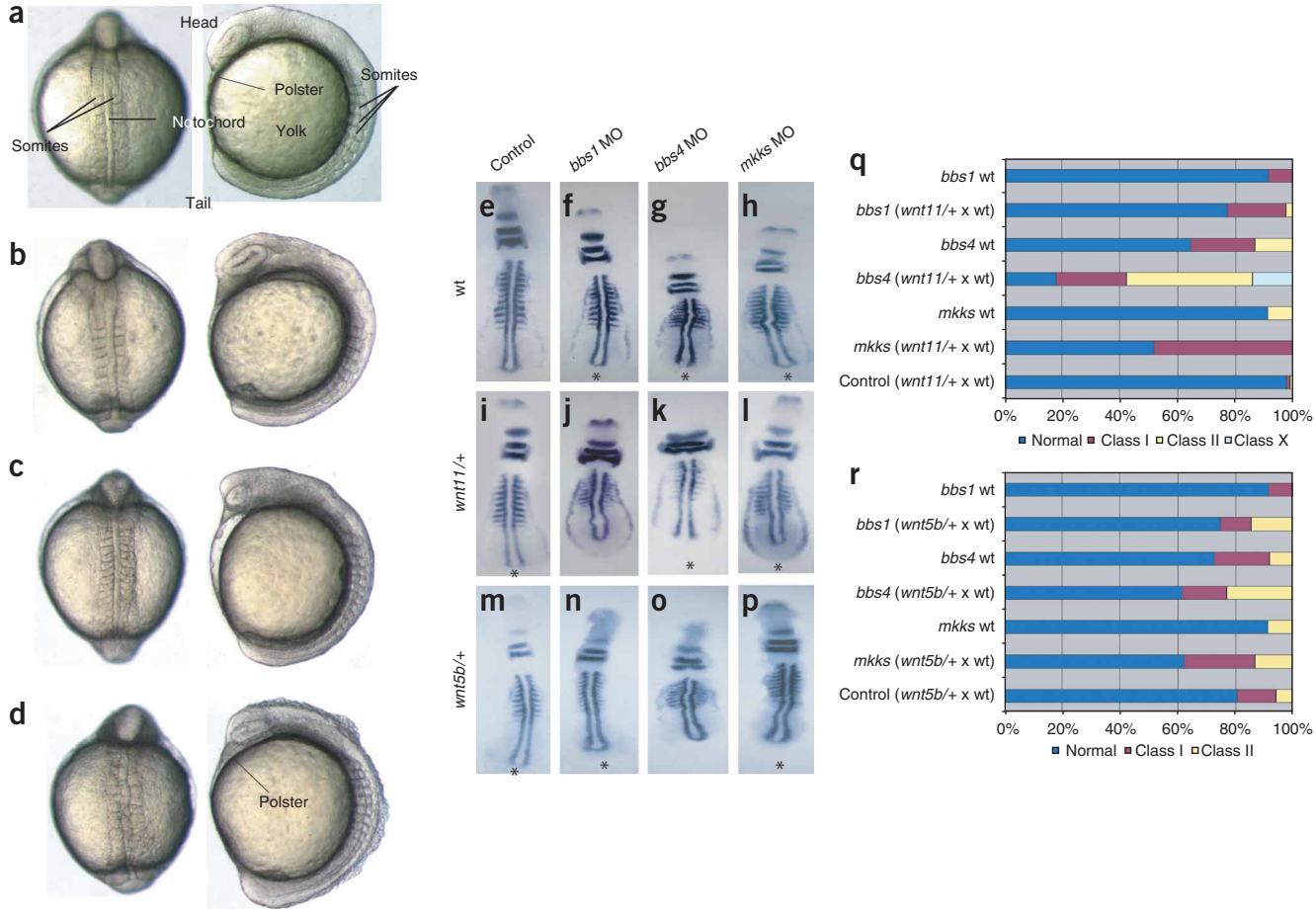

Figure 1 The convergent extension phenotypes of *bbs1, bbs4* and *mkks* morphants. (**a**,**b**) Representative examples of somite stage-matched WT (**a**) and mildly to moderately affected (class I) morphants; *bbs1* morpholino shown (**b**). (**c**,**d**) Representative examples of the phenotypes produced by morpholinos on *wnt11* and *wnt5b* background: *bbs1* morpholino on *wnt11* (**c**) and *bbs4* morpholino on *wnt5b* (**d**, class II). Note the poor definition and aberrant formation of somites and the slight crimping and thickening of the notochord. There is also irregular bubbling up of cellular material from the dorsal side of one of the embryos (**d**). Embryos with irregularly shaped somites and slightly widened notochords were grouped into the mildly to moderately affected class I. Class II embryos were more severely affected and showed severely kinked and widened notochords and substantially shortened body axis. (**e–p**) *Pax2*, *myoD* and *krox20* digoxin-labeled expression in $wnt11^{+/-}$ and $wnt5b^{+/-}$ *bbs1, bbs4* and *mkks* morphants. Morpholinos on WT (**e–h**), *wnt11* (**i–l**) and *wnt5b* (**m–p**) genetic background. Asterisks indicate aberrant posterior *myoD* staining indicative of convergent extension defects[20]. On a WT background, *bbs4* morphants were most severely affected, manifested in poorly defined and irregularly shaped somites, slightly widened notochord in mild to moderate phenotypes (class I) or severely kinked and widened notochord and substantially shorter body axes in the more severely affected specimens (class II). Moreover, in the more severe embryos, we found a 30–50% reduction of the distance between the third rhombomeres and the first somite. For all injected morpholinos in *wnt11/+* outcross, we also found the polster region to be thinner along the body axis and elongated along the dorsal-ventral axis in the severely affected embryos (**i–l**). Somites in morphants were asymmetrically shaped, an effect that was most pronounced in the *bbs4* morphants (**g**,**p**). In addition to the asymmetric shape, somites were also ill-defined, thinned and elongated along the mediolateral axis. Both *bbs4* and *mkks wnt5b*/+ outcross morphants showed undulated notochords (**o**,**p**). All images were taken at ×10 magnification. Embryos shown were identified as heterozygous for *wnt11* or *wnt5b,* respectively. (**q**,**r**) Quantitative representation of the effect *of bbs1, bbs4* and *mkks* morpholinos on *wnt11* and *wnt5b* outcross background. The fractions of embryos of each class are noted in percent along the *x*-axis.

Table 1 Body gap angles of *bbs1*, *bbs4* and *mkks* morphants on WT, *wnt5b* and *wnt11* genetic backgrounds

	Body gap angle (°)	s.d.	*n*	*t*-test
Wild type	48.3	2.87	4	
wnt5a	66.2	14.74	13	0.03
wnt11	83.7	18.39	15	0.001
bbs1 MO	90.9	14.49	15	2.41×10^{-5}
bbs1 (*wnt5b*)	93.5	14.85	13	8.77×10^{-5}
bbs1 (*wnt11*)	112.4	17.21	5	0.0018
bbs4 MO	112.1	19.42	8	7.92×10^{-5}
bbs4 (*wnt5b*)	98.9	19.57	13	6.90×10^{-5}
bbs4 (*wnt11*)	104.7	11.79	11	0.02
mkks MO	80.2	22.11	14	0.012
mkks (*wnt5b*)	94.2	15.63	11	0.00018
mkks (*wnt11*)	110.0	13.74	12	3.60×10^{-5}
bbs1 rescue	46.5	4.51	6	0.51
bbs4 rescue	51.4	7.04	7	0.42
mkks rescue	59.5	10.5	8	0.066
myr/pal *dvl*	51.2	6.10	14	0.37
wnt3a	97.4	30.64	9	0.0096

MO, morpholino.

older embryos (data not shown) and was reminiscent of defects characteristic of other PCP mutants[20]. Overall, the *bbs4* morpholinos produced the most severe phenotype, with an increase of the average gap angle at 9 (±1) somites (**Supplementary Fig. 1** online) from 48° (WT) to >112°. The *bbs1* and *mkks* morphants showed similar phenotypic characteristics, though less frequently than the *bbs4* morphants (**Fig. 1f**,**h**,**q**,**r**). The gap angles increased from 48° (WT) to 90° (*bbs1*) and 80° (*mkks*), respectively (**Table 1**). The morphant phenotypes were rescued by co-injection of morpholino and corresponding RNA, confirming that these phenotypes were caused by the suppression of target translation rather than by a nonspecific effect of the morpholinos (**Table 1**).

Bbs genes interact with non-canonical Wnt mutants

We further examined the requirement for Bbs1, Bbs4 and Mkks in non-canonical Wnt signaling by depleting them in zebrafish embryos with mutations in *wnt11* (also known as silberblick, *slb*) or *wnt5b* (also known as pipetail, *ppt*). Wnt11 and Wnt5b have partially redundant roles in non-canonical Wnt signaling during gastrulation: *wnt11* homozygous mutants manifest convergent extension defects primarily as a failure in the extension of axial tissues[21], and *wnt5b* homozygous mutants have a shortened body axis and defective tail extension[20]. Scoring of >100 embryos showed that injections of 8 ng of *bbs1* morpholino caused only mild (class I) convergent extension defects in <10% of wild-type embryos (**Fig. 1f**,**q**,**r**). In embryos derived from a $wnt11^{+/-}$ outcross, however, the same dose of morpholinos produced convergent extension defects in >20% of embryos (**Fig. 1c**,**j**,**q**). Increasing the *bbs1* morpholino dose to 12 ng in a $wnt11^{+/-}$ genetic background (both inter- and outcross) resulted in a new class of severely affected embryos (**Supplementary Fig. 2a**,**b** online), which were confirmed to be $wnt11^{+/-}$ embryos ($n = 12$, data not shown). Injection of low doses of *bbs4* morpholino into the $wnt11^{+/-}$ outcross resulted in increased lethality, as compared to WT embryos, and defects in 90% of embryos (compared to 37% in WT, **Fig. 1k**,**q**), among them a new, severely affected group of embryos that failed to complete epiboly (**Fig. 1q**, **Supplementary Fig. 2c**). The phenotypes caused by *mkks* depletion in the setting of reduced *wnt11* were strongly enhanced compared to those in WT embryos (**Fig. 1h**,**l**,**q**).

Similarly, antisense depletion of *bbs1*, *bbs4* and *mkks* enhanced the mild convergent extension defects seen in *wnt5b* mutants (**Fig. 1d**,**r**). The effect of *bbs1* depletion in the setting of reduced *wnt5b* function was the least pronounced among the effects of the three genes, as it had been the $wnt11^{+/-}$ setting. All observed phenotypes were consistent with the convergent extension defects of several other zebrafish mutants, indicating that basal body dysfunction may perturb gastrulation movements.

To directly investigate this possibility, we injected a fluorescent lineage tracer into a single marginal blastomere at the 16-cell stage (**Fig. 2**). At 30% epiboly, we observed no differences in cell position and distribution between control injected and morphant embryos (data not shown). However, when we continued observation through to 75% epiboly, movement defects became pronounced (**Fig. 2a**,**b**,**d**). In control embryos, cells converge upon the dorsal midline and, simultaneously, the dorsal axis extends as the arc of cells elongates through gastrulation (**Fig. 2a**). By contrast, embryos injected with morpholinos for *bbs1* (**Fig. 2b**), *bbs4* (**Fig. 2d**) or *mkks* (data not shown) showed defective dorsolateral movements: cells did not converge normally toward the midline. Further, these embryos had deficient extension phenotypes due to substantial alteration of the arc of cells extending along the dorsal axis (**Fig. 2b**,**d**). To confirm that co-injection of *bbs1*, *bbs4* or *mkks* morpholino and WT RNA fully rescues the corresponding convergent extension phenotype, we observed lineages of labeled blastomeres through the stages of gastrulation. In each case, cell movement during gastrulation was also rescued (**Fig. 2c**,**e**): cells moved toward the dorsal midline, and cells that extended along the dorsal axis traveled at a rate similar to those in uninjected controls.

Given the direct relationship between canonical and non-canonical Wnt signaling[22], we considered whether canonical Wnt signaling might also be perturbed in our *bbs1*, *bbs4* and *mkks* morphants by investigating the expression domain of *axin2*, which encodes a downstream target of β-catenin[4,5]. In *bbs1* morphants, the domain of *axin2* expression was expanded compared to that of WT embryos. Most notably, the expression in the tail region was substantially greater than in controls (**Fig. 2f**,**g**). Similarly, *bbs4* and *mkks* morphants showed an expanded *axin2* domain in the tail region (**Fig. 2h**,**i**). To quantify this objectively, we carried out two independent experiments. First, we measured the size of the *axin2* domain with respect to the total body size (because the morphants are shortened, which biases absolute numbers). Blinded measurements of multiple embryos ($n > 10$ per injection) showed that the ratio of the *axin2* domain to body length increased from 8.9% in control embryos to 17.7% in *bbs1* morphants ($P < 0.001$), 16.3% in *bbs4* morphants ($P < 0.001$) and 14.0% in *mkks* morphants ($P < 0.004$). Second, we quantified the message levels of *axin2* as well as *sp5l*, another transcriptional β-catenin target[23], in individual morphant embryos. Although our data were only borderline significant for *bbs4* morphants, most likely because of substantial variability introduced by the very short embryo size and the proportionately marginal amounts of mRNA obtained from each embryo, we found significant (twofold) upregulation of *axin2* in *bbs1* and *mkks* morphants ($P < 0.003$ and $P < 0.05$; **Fig. 2j**), in good agreement with the *in situ* data for *axin2* (**Fig. 2f–i**). We obtained similar results for *sp5l* ($P < 0.009$ and $P < 0.05$; **Fig. 2k**), which, together with our *in situ* data, suggest a concomitant upregulation of Wnt signaling and loss of non-canonical Wnt signaling in *bbs1*, *bbs4* and *mkks* morphants. In addition, we probed the morphants at 50% epiboly for expression of the dorsalization marker *chordin* (*chd*),

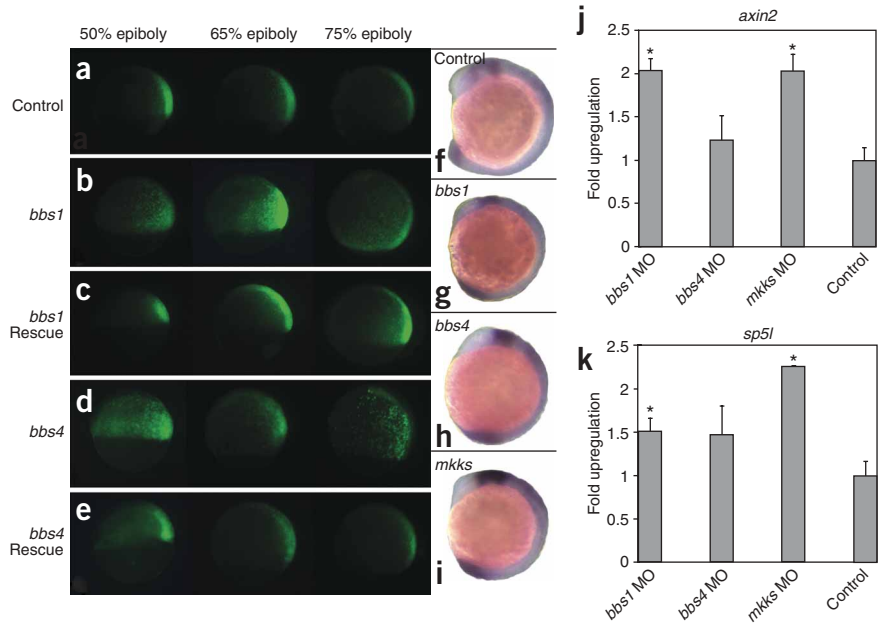

Figure 2 Dysregulation of Wnt signaling in zebrafish morphants. (**a**) Cells descendant from lineage-tracer injected blastomeres at gastrulation converge on the dorsal midline and extend along the anteroposterior axis in control embryos. (**b**–**e**) Cell movement is delayed in embryos injected with *bbs1* morpholino (**b**) or *bbs4* morpholino (**d**) and is rescued by mRNA co-injection (**c**,**e**). (**f**–**i**) The domains of expression of *axin2*, a downstream target of canonical Wnt-signaling, are slightly expanded. Notably, the *axin2* expression domain is expanded in the tail of *bbs1* (**g**), *bbs4* (**h**) and *mkks* (**i**) morphants. (**j**,**k**) Gene expression analysis of β-catenin transcriptional targets *axin2* and *sp5l*. For both *bbs1* and *mkks* morphants, *axin2* and *sp5l* are significantly upregulated. $*P < 0.05$, error bars, s.d.

which is under transcriptional control of β-catenin[24,25]. In WT embryos injected with *bbs4* morpholino, the expression domain of *chd* was expanded with respect to control embryos (**Supplementary Fig. 3b**,**d** online). *Bbs1* morphants shows similar expansion, and the effect was least pronounced in *mkks* morphants (**Supplementary Fig. 3a**,**c**).

Membrane-bound Dvl ameliorates the BbS morphant phenotypes

Subcellular distribution of Dvl is known to be critical for both canonical and non-canonical Wnt signaling. Although cytoplasmic and nuclear Dvl are required for canonical Wnt signaling, membrane-bound Dvl can indicate non-canonical signaling[6,7]. Given that we observed phenotypes consistent with suppressed non-canonical signaling and gene expression data indicative of elevated canonical Wnt signaling, we speculated that enrichment for membrane-bound Dvl might favor enhanced non-canonical signaling and ameliorate the convergent extension phenotype.

Consistent with this hypothesis, we found that introduction of membrane-bound Dvl partially rescued *bbs4* and *mkks* morphant phenotypes. Co-injection of 8 ng of *bbs4* morpholino (which gave rise to severe convergent extension phenotypes in ~80% of embryos) with 50 pg of *Dvl* mRNA carrying both myristoylation and palmitoylation signals for membrane targeting (*myr/pal Dvl*) decreased the number of affected morphants to 58%, a significant improvement ($P < 0.03$, $n = 117$), and co-injection of the same amount of *myr/pal Dvl* with 10 ng of *mkks* morpholino decreased the number of affected morphants from 30% to 14% ($P < 0.02$, $n = 108$). Moreover, the body-gap angle of the rescued embryos (51°) was indistinguishable from that of WT embryos (48°, $P = 0.37$, **Table 1**).

Basal body perturbation and Wnt defects in mammalian cells

To explore the potential role of the basal body and cilium in the regulation of Wnt signaling in mammalian biology, we investigated the effect of *BBS4* suppression in human cells *in vitro*, because *bbs4* morphants showed the most severe convergent extension defect in zebrafish. First, we established that cultured human embryonic kidney (HEK 293T) cells bear a primary cilium and that a substantial subpopulation is indeed ciliated under the experimental conditions used in our studies. Cell stains for γ- and acetylated tubulin and transmission electron microscopy showed one cilium per cell (**Fig. 3a**–**d**), an observation that was consistent for all cells not undergoing mitosis, irrespective of the confluence of the culture. Critically, treatment of cells with vinblastine, which blocks microtubule formation by inhibiting tubulin polymerization, eliminated the cytoplasmic microtubule network but left the primary cilia intact (**Fig. 3e**–**m**), confirming previous studies in protists indicating that microtubule depolymerizers, such as colchicine, do not dissolve already formed cilia[26] and providing us with a tool to discriminate between potential cytoplasmic and ciliary functions of the basal body.

We first tested the responsiveness of ciliated HEK 293T cells to Wnt stimulation using 293T Super8XTOPFlash reporter cells[27], in which firefly luciferase is regulated by eight TCF/LEF1 binding sites and is therefore an indicator of upregulated β-catenin activity (**Fig. 4**). Because WT and BBS-depleted 293T cells were inducible only by Wnt1 and Wnt3a in a panel of Wnt1 through Wnt7b (data not shown), we focused our investigation on Wnt3a-stimulated cellular responses. In a triplicate series of experiments using short hairpin RNAs (shRNAs)[28], we tested the effect of the loss of *BBS1*, *BBS4* and *MKKS* on canonical Wnt signaling. In naive cells transfected with empty vector and reporter control, we observed minimal TCF1/LEF1 activity, which was upregulated by 25–30-fold upon stimulation with Wnt3a. By contrast, transfection of cells with shRNA against *BBS4* resulted in a modest but noticeable increase in basal TCF1/LEF1 transcriptional activity in naive cells, and Wnt3a stimulation resulted in a >120-fold upregulation with respect to unstimulated WT cells transfected with empty vector, and a 3–5-fold upregulation compared to stimulated wild type cells. The phenotype was rescued by coexpression of mouse *Bbs4* cDNA, which escapes suppression by the human shRNA construct (**Fig. 4a**); overexpression of *BBS4* had no effect (data not shown).

Suppression of *MKKS* yielded a similarly pronounced phenotype, with a 2–3-fold increased basal TCF1/LEF activity in naive cells and a >130-fold upregulation in stimulated cells. Notably, *BBS1* suppression did not lead to a statistically significant increase in basal luciferase activity in naive cells but yielded a >110-fold increase upon Wnt3a stimulation (**Fig. 4a**). These data raise the possibility that the basal body can influence the transcriptional activity of β-catenin through two mechanisms, one Wnt dependent and one most likely Wnt independent. Furthermore, the observed effect was indeed a result

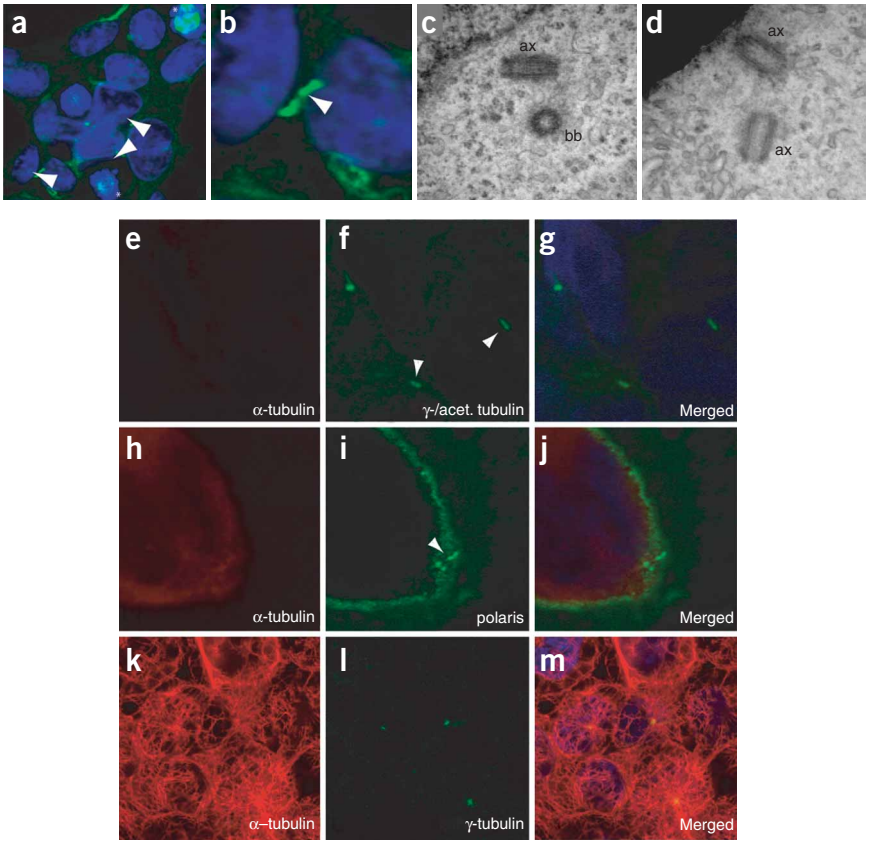

Figure 3 HEK 293T cells are ciliated. (**a**) Cilia in a subconfluent (~70% confluency) culture, as indicated by the acetylated tubulin staining (green). (**b**) Higher magnification of cells from image **a**. (**c**) Transmission EM images from 70% confluent HEK 293T cell cultures showing a basal body with its characteristic 9+0 arrangement and a cross-section of the ciliary axoneme. (**d**) A more superficial plane of HEK 293T cells showing a single cilium intersecting the scanning plane twice; magnification ×70,000. (**e**–**m**) The cytoplasmic microtubule network (**e**,**g**,**h**,**j**), but not the ciliary axoneme (**f**,**g**,**i**,**j**), is disrupted after 6 h of treatment with 100 μM vinblastine compared to untreated cells (**k**–**m**). Staining with anti–α-tubulin as a microtubule marker shown in red (**e**,**h**,**k**), staining with a mixture of antibodies against γ- and acetylated tubulin (centrosomal and ciliary marker) (**f**), anti-polaris/IFT 88 (ciliary marker) (**i**) and anti–γ-tubulin (centrosomal marker)(**l**) shown in green. All images were taken at ×100 magnification.

of altered TCF/LEF1 transcription, as a control experiment with the mutant pFOPFlash reporter[29] did not lead to increased luciferase activity (data not shown).

In addition to disruption of basal body and ciliary function, a hallmark of *BBS4* suppression is disruption of the microtubular network[28]. To probe whether increased luciferase activity was related to loss of cytoplasmic microtubule organization or ciliary dysfunction, we interfered chemically with the organization of cytoplasmic microtubules. Treating HEK 293T cells with paclitaxel (Taxol), a microtubule stabilizer, did not change the luciferase activity in either unstimulated or stimulated cells (**Fig. 4c**). Notably, treatment with vinblastine did not alter the Wnt3a response of cells that were ciliated but had a perturbed cytoplasmic microtubule network (**Fig. 3e–j**).

Next, we reasoned that if ciliary function is required for eliciting Wnt response, disruption of intraflagellar transport should phenocopy the *BBS1*, *BBS4* and *MKKS* suppressants. To test this hypothesis, we suppressed *KIF3A*, an axonemal-specific kinesin motor whose loss causes complete shutdown of cilium assembly and maintenance[30]. Using two non-overlapping shRNAs against human *KIF3A*, each of which results in >80% message suppression (data not shown), we observed that the phenotype of *KIF3A* suppressants closely resembled that of cells with suppressed *BBS1, BBS4* and *MKKS* (**Fig. 4b**), suggesting that the cilium and intraflagellar transport are necessary for modulating β-catenin–associated transcription.

Biochemical basis of the Wnt defect

To probe the biochemical basis of the luciferase phenotype, we examined the distribution and accumulation of β-catenin and DVL1 and DVL3 (two of the three known mammalian isoforms of DVL for which suitable antibodies are available) in the cellular compartments of HEK 293T cells. Consistent with our earlier data, we observed that upon *BBS4* suppression, β-catenin accumulation (standardized against a GAPDH internal control, which has known discrete cytoplasmic and nuclear isoforms[31]) increased 1.5-fold in cytoplasmic and 1.4-fold in nuclear protein fractions compared to that in cells treated with empty vector (**Fig. 4d**). However, membrane-bound β-catenin remained unaltered. Similarly, levels of DVL1 were higher in *BBS4* than in controls (by 2.0-fold in cytoplasmic and 1.5-fold in nuclear DVL1). Notably, we found DVL3 in the nuclear protein fraction upon suppression of *BBS4* (54-fold upregulation), whereas we saw no appreciable nuclear DVL3 in cells treated with empty vector, other than trace amounts that likely reflect modest fractionation impurities.

Previous studies have postulated that nuclear localization of DVL is necessary for canonical Wnt signaling[32]. Notably, we found that not only does suppression of *KIF3A* phenocopy *BBS4* depletion with regard to β-catenin, but the phenotype is more acute, which is consistent with the greater upregulation of TCF1/LEF1 transcriptional activity in *KIF3A* suppressants compared to *BBS4*-silenced cells (**Fig. 4a**,**b**,**e**). When we suppressed nuclear export, but not import, by treatment with *N*-ethylmaleimide (NEM)[32], we found no differences between β-catenin levels in the nuclear and cytoplasmic fractions of either WT or *BBS4*-depleted cells (data not shown). Moreover, we found increased levels of DVL3 in the nucleus of both *KIF3A* and *BBS4* suppressants (**Fig. 4f**) with concomitant decrease of cytoplasmic DVL3 (which is essentially depleted in *KIF3A* suppressants), providing further evidence for increased canonical Wnt signaling upon silencing of both ciliary and basal body proteins. Notably, that phenotype was concurrent with a modest decrease of JNK (**Supplementary Fig. 4**), a marker for non-canonical signaling[7].

BBS4 influences the canonical–non-canonical balance

The Wnt classes of canonical (Wnt1) and non-canonical Wnt signaling (Wnt5a) were originally characterized by their phenotypes[33–35]. In addition, Wnt5a can antagonize and repress β-catenin/TCF/LEF1 transcription, although the mechanism remains unclear[22]. Because the loss of non-canonical signaling in zebrafish and the expansion of *chd* and *axin2*, both indicative of increased transcriptional activation

of β-catenin responsive elements, are consistent with the effects of BBS1, BBS4 and MKKS depletion upon Wnt3a stimulation in 293T cells, we speculated that the loss of basal body function perturbs the antagonistic effects of Wnt5a on Wnt3a signaling. We therefore tested whether overexpression of Wnt3a in zebrafish phenocopies the *bbs1*, *bbs4* and *mkks* morphants. Although injection of high doses of Wnt3a induced dorsalization and double axis formation (data not shown), low Wnt3a doses (10 pg) gave rise to an identifiable convergent extension phenotype: embryos had a significantly shortened body axis (body-gap angle 97°, $P < 0.0096$), a kinked notochord, and broadened and abnormally shaped somites (**Fig. 5a**). Tracking of fluorescently labeled cells during epiboly phenocopied the *bbs1*, *bbs4* and *mkks* morphants (**Fig. 5b**), and expression analysis of *chd* showed a slightly expanded expression domain (**Fig. 5c**).

We then sought to determine whether overexpression of WNT5A in BBS4-depleted HEK cells could rescue the phenotype. In a triplicate series of luciferase experiments, we titrated cells with suppressed BBS4 in the presence or absence of WNT5A with a dilution series of WNT3A-enriched medium (**Fig. 5d**). Consistent with previous studies, we observed that control cells lost the WNT3A response in the presence of WNT5A. However, the cellular response to WNT3A could not be suppressed in cells lacking BBS4. These observations were further substantiated in zebrafish, because the *bbs1*, *bbs4* and *mkks* morphant phenotypes could not be rescued by overexpression of Wnt5a (data not shown). These results suggest that a mild stimulation with canonical Wnt signals can give rise to phenotypes reminiscent of loss of non-canonical Wnt signaling.

Proteasomal defects contribute to β-catenin stabilization

The prevailing phenotype we observed—the presence of excessive β-catenin, primarily in the cytoplasm—is suggestive of deficiencies in β-catenin clearance. To investigate this possibility, we assayed the

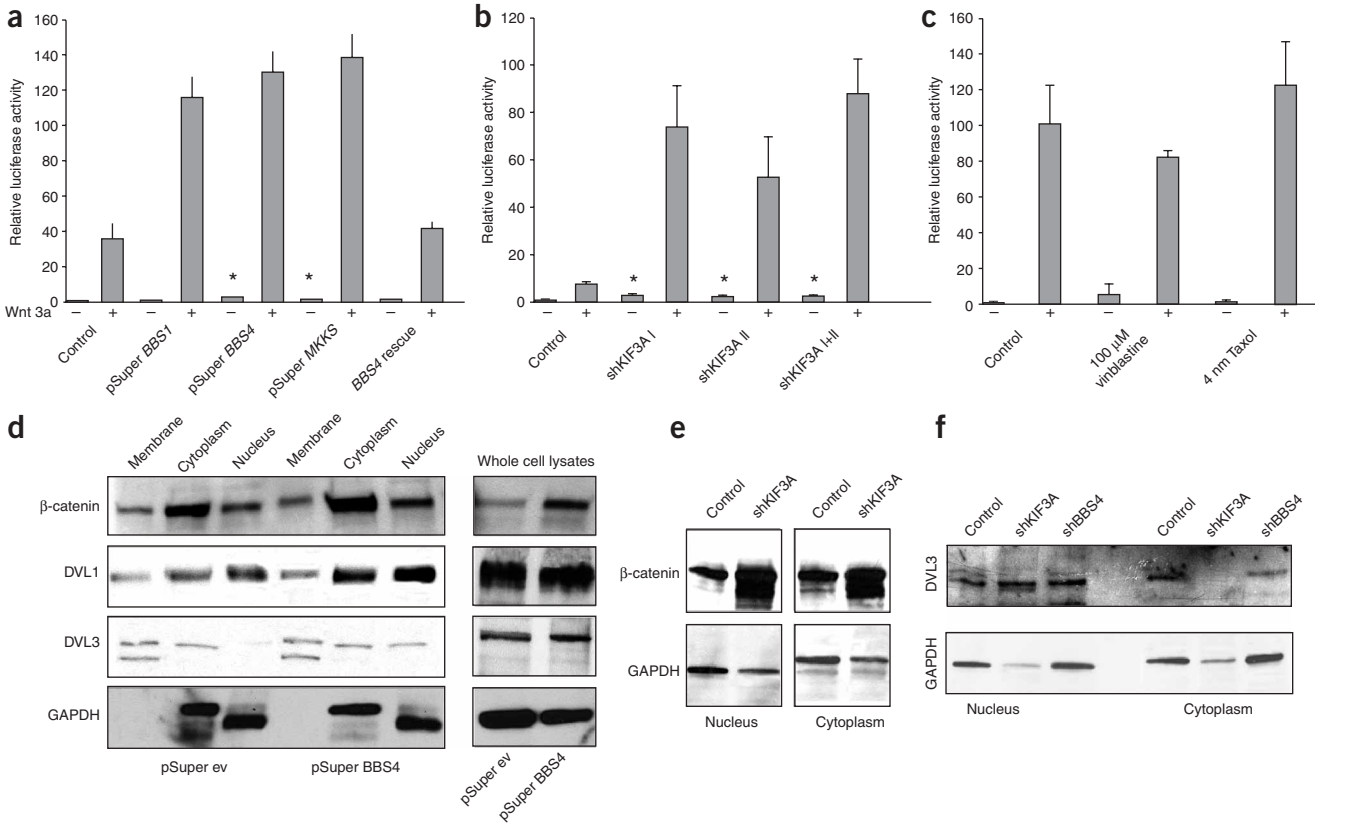

Figure 4 Dissection of the Wnt defect in HEK 293T cells (**a**) Relative luciferase activity in response to active β-catenin upon suppression of *BBS1*, *BBS4* and *MKKS*. The luciferase activity in naive cells without BBS4 is significantly upregulated compared to control; the Wnt response is further augmented. Depletion of MKKS gives rise to a similar phenotype (significant basal upregulation and strongly enhanced Wnt response). Depletion of BBS1 did not lead to elevated luciferase activity in naive cells but yielded a similarly augmented Wnt response. Asterisks indicate a significantly upregulated luciferase activity ($P < 0.05$). The response was normalized to the luciferase activity in unstimulated WT cells. (**b**) Suppression of *KIF3A* phenocopies *BBS4* and *MKKS*-suppressed cells. The basal β-catenin activity is upregulated significantly with either *KIF3A* shRNA and the Wnt response is strongly augmented (asterisks indicate significant upregulation of luciferase activity, $P < 0.05$). (**c**) Disruption (via treatment with vinblastine) or stabilization (via treatment with paclitaxel (Taxol)) of the cytoplasmic microtubular network do not alter the Wnt response significantly. Error bars (**a**–**c**), s.d. (**d**) Increased cytoplasmic and nuclear β-catenin levels in *BBS4* suppressants. HEK 293T cells transfected with pSuper BBS4 plasmid show upregulation of cytoplasmic (1.5-fold) and nuclear (1.4-fold) β-catenin levels compared to control. Similarly, the cytoplasmic and nuclear fraction of DVL1 protein (85 kDa) is increased (2.0- and 1.5-fold, respectively). DVL3 (90 kDa) shows nuclear localization in BBS4-deficient cells but not in the control (>54-fold upregulation). The levels of both DVL1 and DVL3 in whole-cell lysates are comparable in WT and BBS4 depleted cells. The meaning of the lower-molecular-weight membrane DVL3 band is unclear; it may reflect an unknown DVL3 isoform. GAPDH was used as a control. Quantification was carried out by image analysis. (**e**) The phenotype resulting from loss of *BBS4* can be recapitulated by suppression of *KIF3A*. Both cytoplasmic and nuclear levels of β-catenin are elevated when *KIF3A* is suppressed. (**f**) Blocking of nuclear export shows increased DVL3 protein in the nucleus of both *KIF3A* and *BBS4* suppressants. Nuclear DVL3 is elevated and cytoplasmic protein is depleted in both *BBS4* and *KIF3A* suppressed cells.

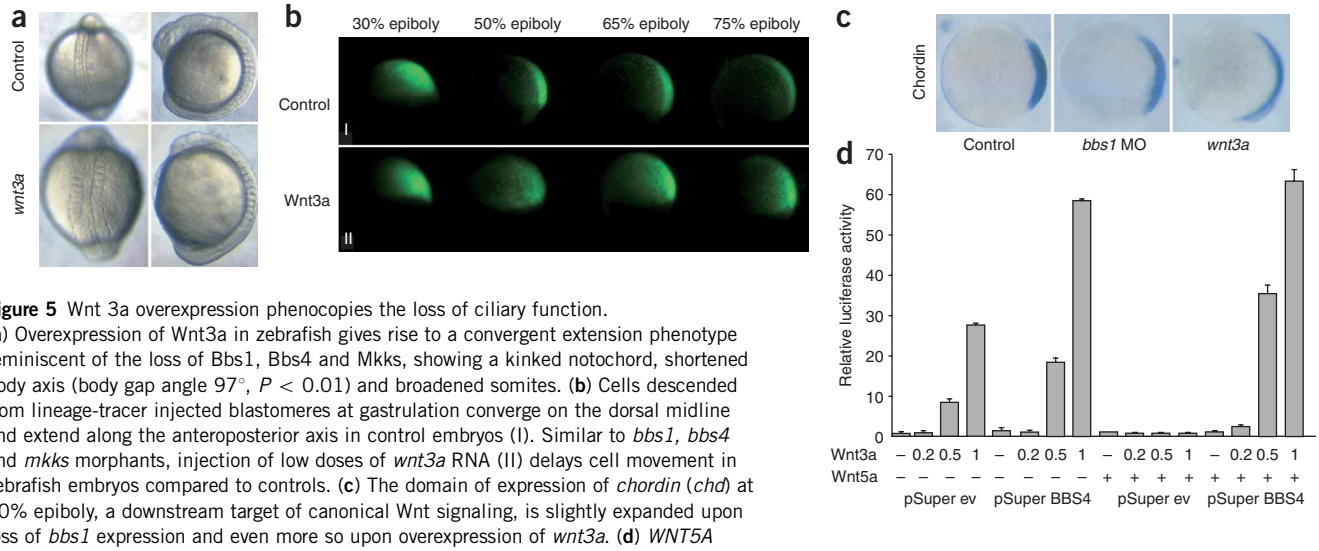

Figure 5 Wnt 3a overexpression phenocopies the loss of ciliary function. (**a**) Overexpression of Wnt3a in zebrafish gives rise to a convergent extension phenotype reminiscent of the loss of Bbs1, Bbs4 and Mkks, showing a kinked notochord, shortened body axis (body gap angle 97°, $P < 0.01$) and broadened somites. (**b**) Cells descended from lineage-tracer injected blastomeres at gastrulation converge on the dorsal midline and extend along the anteroposterior axis in control embryos (I). Similar to *bbs1, bbs4* and *mkks* morphants, injection of low doses of *wnt3a* RNA (II) delays cell movement in zebrafish embryos compared to controls. (**c**) The domain of expression of *chordin* (*chd*) at 50% epiboly, a downstream target of canonical Wnt signaling, is slightly expanded upon loss of *bbs1* expression and even more so upon overexpression of *wnt3a*. (**d**) *WNT5A* overexpression in 293T cells cannot rescue the phenotype caused by the suppression of *BBS4*. Although luciferase activity in response to a dilution series of WNT3A enriched medium is suppressed upon *WNT5A* overexpression in control cells, it remains unaltered upon suppression of *BBS4*. Error bars, s.d.

stability of β-catenin in *BBS4* suppressants by evaluating the total accumulation of the protein in cells pulsed with ^{35}S-methionine, followed by immunoprecipitation (IP) with a β-catenin–specific antibody (anti–β-catenin). A 60-min time-course study showed progressive, pronounced accumulation of both phosphorylated and unphosphorylated protein (**Fig. 6a**), raising the possibility that both clearance and phosphorylation were perturbed upon disruption of the basal body. Given the recent demonstration that at least one of the human BBS (Bardet-Biedl syndrome–associated) genes encodes a putative ubiquitin ligase (*BBS11*)[36], together with the known enrichment of the proteasome in the pericentriolar region[37], we hypothesized that suppression of *BBS4* might lead to defects in proteasome function. To test this, we assayed proteasome activity using a reporter cell line in which green fluorescent protein (GFP) is tagged with mouse ornithine decarboxylase (OCD) with a proteasomal targeting sequence for both ubiquitin-dependent and independent degradation. In contrast to cells transfected with empty vector, in which we observed minimal fluorescence, cells transfected with *BBS4* shRNA showed a pronounced GFP signal, reminiscent of fields of cells treated with proteasome inhibitors such as acetyl-L-leucyl-L-leucyl-L-norleucinal (ALLN) and lactacystin (**Fig. 6b**). To quantify this phenotype, we flow-sorted cells and measured total luminescence, and we observed significant GFP activity indicative of perturbation, but not complete ablation, of proteasomal function (**Fig. 6c**). Notably, the lack of efficient degradation of GFP was not due to defective ubiquitination, because immunoprecipitation of GFP in either control or *BBS4* suppressant cells and probing with ubiquitin revealed no differences (data not shown). In addition, the core activity of the proteasome was likewise normal: real-time monitoring of the degradation of synthetic peptide Suc-LLVY-AMC in cell extracts[38] showed no differences between control and suppressant cells (**Supplementary Fig. 5**).

Given these observations, we considered the possibility that proteasomal targeting of β-catenin in a BBS4-dependent fashion might be defective. We therefore tested whether BBS4 can interact with any subunits of the proteasome. Using a combination of yeast two-hybrid analysis and co-immunoprecipitation, we observed that BBS4 interacted specifically with RPN10, a 26S subunit (**Fig. 7a–c**), but not with any barrel or lid proteins tested, including the 20S subunits α1, α2, α3, α5, α6 and α7 as well as RPN12, RPN2, RPN7 and RPT6 (data not shown). These data suggested that RPN10-dependent targeting might be causally related to the observed defects, especially because RPN10 is the best-characterized proteasome subunit with ubiquitin recognition motifs[39,40]. We reasoned that if this is was the case, suppression of the gene *RPN10* should phenocopy the aberrant TCF1/LEF1

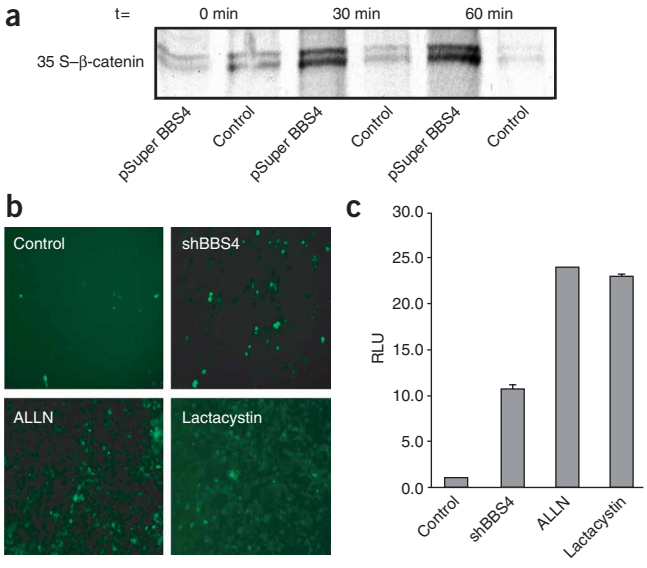

Figure 6 Proteasomal protein degradation is impaired in *BBS4*-silenced cells. (**a**) ^{35}S-labeled β-catenin is stabilized in *BBS4*-depleted HEK 293T cells compared to controls. After 30 and 60 min, both phosphorylated (upper band) and unphosphorylated (lower band) forms of β-catenin are substantially enriched with respect to control transfected cells. (**b**,**c**) Defective proteasome function upon loss of *BBS4* and treatment with two known proteasome inhibitors, ALLN and lactacystin. The amount of green fluorescence is increased as indicated by fluorescence microscopy (**b**) and quantified by fluorescence activated cell sorting (**c**). Error bars, s.d.

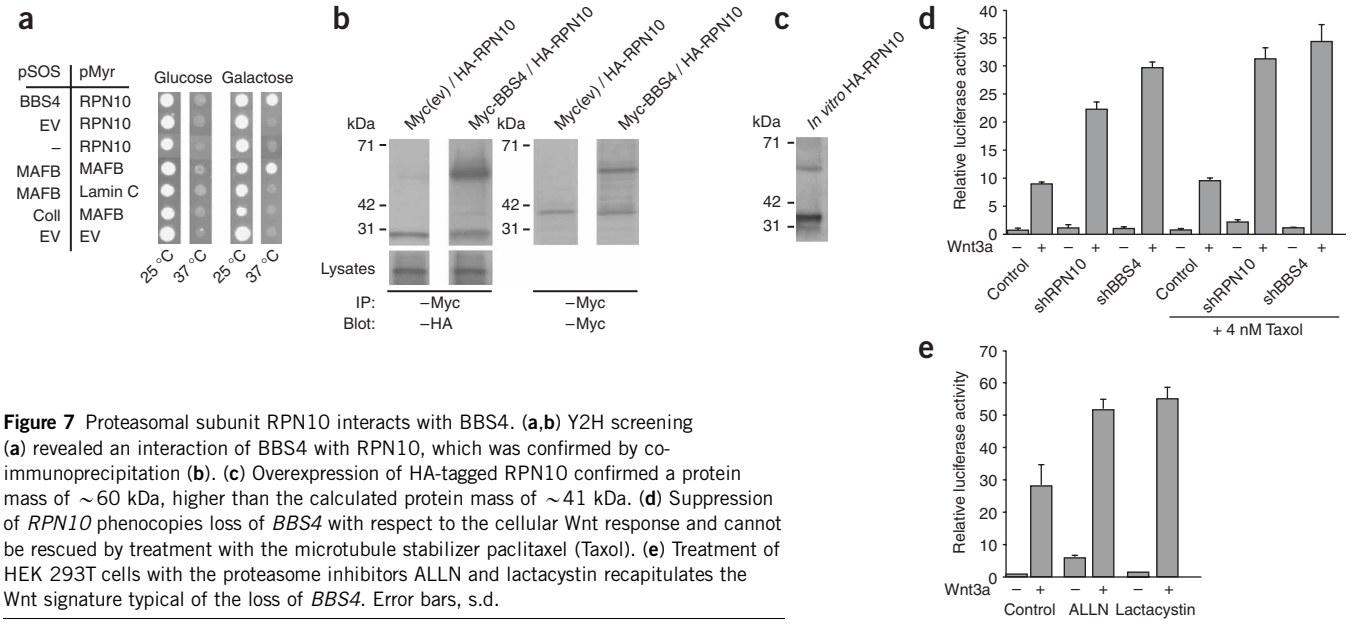

Figure 7 Proteasomal subunit RPN10 interacts with BBS4. (**a**,**b**) Y2H screening (**a**) revealed an interaction of BBS4 with RPN10, which was confirmed by co-immunoprecipitation (**b**). (**c**) Overexpression of HA-tagged RPN10 confirmed a protein mass of ~60 kDa, higher than the calculated protein mass of ~41 kDa. (**d**) Suppression of *RPN10* phenocopies loss of *BBS4* with respect to the cellular Wnt response and cannot be rescued by treatment with the microtubule stabilizer paclitaxel (Taxol). (**e**) Treatment of HEK 293T cells with the proteasome inhibitors ALLN and lactacystin recapitulates the Wnt signature typical of the loss of *BBS4*. Error bars, s.d.

transcriptional activation seen in BBS4-suppressed cells. A Super8-xTOPFlash assay in cells suppressed for *RPN10* supported this hypothesis (**Fig. 7d**). The Wnt phenotype was also recapitulated by chemical poisoning of the proteasome with two separate inhibitors (**Fig. 7e**), but there was no evidence of rescue of the *RPN10* or *BBS4* suppressant phenotype with paclitaxel, which might be expected to help stabilize cytoplasmic microtubule defects (**Fig. 7d**).

Finally, we noted that the β-catenin defects could not be attributed exclusively to proteasomal dysfunction because of the substantial accumulation of unphosphorylated protein in *BBS4*-suppressed cells. This raised the possibility that phosphorylation or dephosphorylation might be defective. As an initial investigation into this possibility, we examined the recently defined ciliary proteome[41] for known β-catenin kinases and phosphatases and found that both casein kinase 1D (CK1D) and the α subunit of the protein phosphatase-1 complex (PPP1C) were predicted to be involved in ciliary function. Although the details of this involvement will require substantial further investigation, expression of tagged CK1D in HEK 293T cells showed discrete localization of the protein to the centrosome (**Supplementary Figure 6a–c**), and PPP1C localized to the pericentriolar region of HEK 293T cells and to both the centrosome and the basal body of ciliated IMCD3 cells (**Supplementary Figure 6d–i**). Together, these observations suggest that perturbations of these organelles may disturb the function of either or both enzymes.

DISCUSSION

In this study, we have investigated the role of the cilium and basal body in Wnt signaling. We propose that these organelles influence the interpretation of the Wnt signal, with the presence of the cilium, an inherently postmitotic structure, favoring the non-canonical arm of the pathway. Consistent with this notion, suppression of basal body proteins causes PCP defects, and the same proteins can interact genetically with non-canonical Wnt mutants. In parallel, the observed non-canonical Wnt phenotypes also affect canonical Wnt signaling. However, we did not observe pronounced dorsalization of embryos, nor are ciliary disorders typically characterized by hyperproliferative defects, which are often associated with aberrant β-catenin overactivation[42]. These data suggest that attenuated non-canonical signaling is not fully reciprocated by increased canonical signaling, possibly because of downstream checkpoints.

The formal possibility remains that the basal body can perturb canonical and non-canonical Wnt signaling independently. However, several lines of evidence support a reciprocal, but not proportionate, model. First, we observed that overexpression of *WNT5A* suppressed TCF–β-catenin transcriptional activation, which is consistent with previous reports[22,43–46]. Moreover, modest overexpression of *wnt3a* in zebrafish embryos did cause phenotypes reminiscent of *wnt5* loss-of-function mutants, although higher concentrations of Wnt3a induced canonical phenotypes that included dorsalization of embryos and double axis formation, further suggesting a titration effect or competition of the activity of the two ligands. Finally, in mammalian cells, TCF/LEF1-based upregulation was suppressed by overexpressing *WNT5A*, but that function was lost upon disruption of the basal body. This may indicate that the basal body acts downstream of the Wnt ligand, although we favor the possibility that perturbation of the basal body alters the behavior of effector molecules common to both arms of the pathway, such as Dvl, ultimately desensitizing the cell to a signal switch. Indeed, we were able to partially rescue the *bbs1*, *bbs4* and *mkks* morphant phenotypes by enriching for membrane-bound Dvl, suggesting that the subcellular distribution and/or regulation of degradation of Dvl might be influenced directly by the function of the cilium and the basal body.

The present studies, as well as previous work showing that inversin, another protein found in basal body and cilia, regulates the degradation of cytoplasmic Dvl[47], are beginning to highlight a potential mechanistic model for observed basal body Wnt defects that are common in *inv*, *bbs1*, *bbs4* and *mkks* mutants and morphants. Our data suggest that the persistence of β-catenin is partially attributable to defective degradation by the proteasome, a complex known to be enriched in the pericentriolar region[37]. The defective degradation is possibly attributable to perturbed interaction of the proteasomal subunit RPN10 with BBS4, although other factors may also be involved. This defect is not specific to the Wnt signaling pathway, a notion consistent with the synthetic phenotypes observed in *bbs1*, *bbs4* and *mkks* morphants, which indicate that convergent extension is only one of several developmental processes disrupted upon the silencing of

these genes. We speculate that the transmission of PCP or other Wnt signals from the cilium is likely to be interpreted at the pericentriolar region and to dictate a range of decisions mediated by the pericentriolar material, including proteasomal degradation, phosphorylation and dephosphorylation (at least one kinase and one phosphatase localize primarily in this cellular region) and possibly proteolytic cleavage. Notably, the vertebrate primary cilium has been implicated in a number of other signaling pathways[48], and it is conceivable that basal body–mediated processing of key downstream effector components are important in the interpretation of those signals.

METHODS

Morpholinos and embryo manipulations. Translational morpholinos against *bbs1*, *bbs4* and *mkks*, and a control morpholino, were designed by and obtained from Gene Tools, LLC. We injected 1 nl of diluted morpholino into WT zebrafish embryos at the 1- to 2-cell stage. Injected embryos were observed for 24–30 h and then scored. For RNA rescue experiments, *bbs1*, *bbs4* and *mkks* mRNA were transcribed *in vitro* using the SP6 Message Machine kit (Ambion). We classified morphant embryos into two graded phenotypes on the basis of the relative severity compared with age-matched controls from the same clutch, as evaluated by two independent investigators blinded to the experiments. On mutant outcross backgrounds, we injected 8 ng of *bbs1* morpholino, 3.5 ng of *bbs4* morpholino and 3.0 ng of *mkks* morpholino, respectively.

Morphometric analyses and classification of zebrafish embryos. For morphometric analyses, embryos were picked randomly and analyzed at 8–10 somites. We ran a *t*-test to determine the significance of different body gap angles. We grouped the embryos into four classes. Class I embryos were mildly to moderately affected and displayed a shortened body axis, mediolaterally elongated somites and notochord imperfections. Class II embryos were more severely affected, as defined by severely shortened body axes, bubbling of cells, mediolaterally elongated somites, and widened and kinked notochord. Class X embryos were observed for injections of *bbs4* morpholino on various backgrounds. They did not finish epiboly, and the yolk sac frequently disintegrated. Class Y embryos received *bbs1* morpholino injections at high concentrations and were defined by extremely mediolaterally elongated somites, severe notochord kinks, an ovoid shape of the embryo and other abnormalities.

Whole-mount RNA *in situ* hybridization and microscopy. Embryos for *in situ* hybridization were fixed overnight in 4% paraformaldehyde/PBS. We carried out whole-mount *in situ* hybridization according to standard protocols using digoxygenin-labeled antisense RNA probes synthesized by *in vitro* transcription (Roche). We applied *chd*, *axin2*, and *pax2/krox20/myoD* (mix) riboprobes to embryos at a concentration of 0.5–1.0 ng/μl[49]. We obtained images of embryos processed for *in situ* hybridization using a Zeiss Axioplan 2 microscope in conjunction with a Zeiss AxioCam digital camera.

Monitoring of gastrulation movements. To determine how convergent extension movements are altered at gastrulation stages, we injected a single marginal blastomere in morpholino-injected and uninjected control embryos at the 16-cell stage with 1 nl of 10,000-MW dextran-conjugated green fluorescent lineage tracer (Invitrogen/Molecular Probes). We began our observation at 30% epiboly in embryos with fluorescent clones in the dorsal region. At early, mid and late epiboly stages of live embryos, we observed the position of fluorescent cells to monitor how cells move toward the midline of the embryo and extend along the anteroposterior axis.

Protein blots. We transfected HEK 293T cells at ~70% confluence with Polyfect (Qiagen) and blocked nuclear export as described[32]. Cells were harvested 72 h after transfection: the membrane protein fraction was isolated with the Mem-PER protein preparation kit (Pierce), cytoplasmic and nuclear fractions were isolated with the NE-PER kit (Pierce) and whole-cell lysates were obtained by lysis with modified RIPA buffer (150 mM sodium chloride, 50 mM Tris-HCl, pH7.4, 1% Nonidet P-40, 0.1% sodium deoxycholate, 1 mM EDTA). Protein content was measured by the Lowry method and samples were normalized. 20 μg of total protein was separated by SDS-PAGE on precast Rgels (10% or 4–15% Tris-HCl) and transferred to a PVDF membrane (Bio-Rad). The membrane was probed with commercial antibodies raised in rabbit (anti–β-catenin (1:100, Santa Cruz SC7199), anti-Dvl1 and anti-DVl3 (both 1:500, Chemicon AB5970 and AB5974, respectively), and JNK/SAPK1 (1:1,000, Upstate cat. no. 06-748)) and in mouse (anti-GAPDH (1:5,000, Abcam ab 9894)). Proteins were detected with secondary antibodies conjugated to horseradish peroxidase (1:10,000 each, RPN4201 and RPN4301) and the ECL detection kit (both GE Healthcare).

Luciferase reporter system assays. We carried out experiments with HEK 293T cells (pTOPFlash/pFOPFlash), HEK 293T cells stably expressing pTOPFlash reporter (BBS, KIF3A depletion, stimulation with Wnt1–Wnt7b) or HEK 293T cells stably expressing both pTOPflash and *Renilla reniformis* luciferase control plasmid pRL SV40 (vinblastine, paclitaxel, proteasome inhibitors). Cells were seeded in 24-well plates at a density of 10^4 cells per well. After 18–24 h, we transfected six wells of each plate with reporter plasmid and/or *Renilla* luciferase cDNA in an SV40 vector and the plasmid of interest using the Polyfect (Qiagen) optimized transfection protocol. We used Super8xTOPFlash[27] and pRL SV40 (*Renilla* luciferase) as an internal control, pFOPFlash[29] to ensure TCF/LEF1 transcriptional specificity, pSuper BBS4 (ref. 28), pSuper BBS1 and pSuper BBS6 (our unpublished data), shRNA constructs targeting KIF3A obtained from Open Biosystems (V2HS_202388 and V2HS_203317) and mouse Wnt1–Wnt7b cDNAs. When applicable, after 24 h we treated three wells of each plate with Wnt3a-enriched medium that had been aspirated from Wnt3a/L cells[50] and sterile filtered before being applied to the luciferase assay. Cells were lysed and luciferase activity measured 48 h after start of stimulation using the Promega Dual Luciferase Reporter Assay System (E1910) and a FluoStar Luminometer (BMG Technologies). For experiments requiring treatment with vinblastine and paclitaxel (Toronto Chemicals), we treated cells with the drugs 24 h after transfection. For Wnt3a stimulation experiments, we removed and pooled media from Wnt3a/L cells, and we diluted the pooled stock with media lacking Wnt3a in a ratio of 1:4 (0.2) or 1:1 (0.5) or administered it undiluted (1). Each assay was repeated at least twice to ensure reproducibility of the results.

Pulse-chase experiments. HEK 293T cells were transfected with pSUPER ev or pSUPER BBS4 at ~70% confluency in 6-cm dishes. At 72 h after transfection, we removed the medium and replaced it with labeling medium lacking both methionine and cysteine and supplemented with dialyzed FBS (Gemini). After 40 min of incubation, we added 50 μl (0.7 mCi) of ^{35}S-labeling mix (Redivue, GE Healthcare) and incubated the cells for an additional 40 min. At the end of the pulse, cells were washed twice with PBS and then were either lysed ($t = 0$ min) with modified RIPA buffer supplemented with protease inhibitor or incubated with normal growth medium for an additional 30–60 min before lysis in modified RIPA buffer. We centrifuged the lysates at 16,000*g* and 4 °C for 10 min and removed and incubated the supernatants with anti–β-catenin (rabbit, Santa Cruz SC-7199) and protein A beads (Sigma) at 4 °C overnight. Beads were washed five times with modified RIPA buffer and boiled in SDS loading buffer (Bio-Rad) for 5 min. We separated the supernatant via SDS-PAGE on a 10% Tris-HCl gel (Bio-Rad), soaked the gels in 10% glycerin in Tris-glycine sodium chloride (TGS; Bio-Rad) for 30 min and dried them on a gel dryer (Savant) at 80 °C for 2 h. The gels were exposed on autoradiography film over 48 h.

Immunocytochemistry. We treated glass cover slips with 0.001% poly-L-lysine to help HEK 293T cells adhere. Cells were seeded onto glass cover slips (untreated for IMCD3, treated for HEK 293T) and transfected at ~70% confluency. We fixed the cells in ice-cold methanol 48 h after transfection at –20 °C for 10 min. After rinsing with PBS (twice), cell membranes were permeabilized using 0.1% Triton-X (American Bioanalytical) in PBS (10 min), washed (PBS, twice), and blocked with 5.5% FBS (Gemini) in PBS for 30 min. Subsequently, cells were washed again (PBS, twice) and incubated with primary antibody at 25 °C. We used anti–γ-tubulin (1:1,000, Sigma T6557), anti–acetylated tubulin (1:1,000, Sigma T6793), anti–α-tubulin (1:1,000, Sigma T6199), anti-polaris (IFT88) and anti-V5 (1:1,000, Invitrogen 46-0705). After incubation, cells were washed (PBS, three times) and incubated with secondary antibody (anti–mouse IgG and anti–rabbit IgG conjugated with AlexaFluor488 and AlexaFluor546, both from Invitrogen) in the dark at 25 °C for 1 h. After

completion, cells were washed (PBS, three times) and incubated with DAPI (1:5,000, 500 mg/ml stock solution) at room temperature for 10 min. Cells were then washed (PBS, three times) and mounted with Prolong Gold Antifade (Invitrogen). We recorded images with a Zeiss LSM 510 confocal microscope in multitrack mode at ×100 magnification.

***In vivo* proteasome activity assay.** We carried out *in vivo* studies of proteasome function using a commercially available HEK 293 ZsGreen proteasome sensor cell line (Clontech) transiently transfected with pSuper ev or pSuperBBS4, or treated with 10 μM ALLN or 5 μM lactacystin, respectively, for 6 h. At 72 h after transfection, 10× fluorescent images of live cells were taken on a Zeiss Axiovert 135TV inverted fluorescence microscope.

Fluorescence-activated cell sorting (FACS). Samples were trypsinized and resuspended in 1 ml PBS buffer with 100 μg/ml BSA (Sigma). Samples were run in triplicate and analyzed with the BD Immunocytometry LSR III system (BD Biosciences).

***In vitro* proteasome activity assays.** We carried out *in vitro* evaluation of proteasome activity by following the hydrolysis and concomitant fluorescence emission of 7-amino-4-methylcoumarin (AMC) from the synthetic peptide Suc-LLVY-AMC (Bachem) as described[38]. HEK 293T cells were either treated with 5 μM lactacystin for 8 h or transfected with the different shRNA-expressing constructs (pSUPER ev, pSUPER BBS4 and pSUPER RPN10) and incubated for 72 h. We harvested cells in Buffer A (20 mM Tris-HCl, 5 mM $MgCl_2$, 1 mM β-mercaptoethanol, 1 mM ATP, 10% glycerol) to assess 26S proteasome activity. We measured protein concentration using the DC protein assay (Bio-Rad). We mixed 20 μl of sample (normalized for protein amounts and performed in triplicate) with 250 μl of 50 μM Suc-LLVY-AMC (in 50 mM Tris-HCl, pH 8.0, and 1 mM β-mercaptoethanol) and recorded emission fluorescence using 360-nm excitation and 460-nm emission wavelengths over a period of 30 min at 37 °C using a Perkin Elmer Wallac 1420 Vector 2 multilabel counter.

Protein-protein interactions. Yeast two-hybrid analysis was carried out as described; screening was performed using the Cytotrap assay (Stratagene) as described[28] and following the manufacturer's instructions. For immunoprecipitations, we cloned the ORFs of both BBS4 and RPN10 into the pCMV-Myc and pCMV-HA mammalian expression vectors (Clontech). Coimmunoprecipitation assays were carried out as described[28].

Note: Supplementary information is available on the Nature Genetics website.

ACKNOWLEDGMENTS

We apologize to our colleagues whose work we were unable to cite because of a strict 50-reference limit. We thank J. Nathans, J. Axelrod, L. Menezes, G. Germino and E. Davis for their critical evaluation of this manuscript, and A. Gherman for the quantification of the western blots. We also thank J. Nathans for the gift of the 293T luciferase reporter cell line, J. Kitajewski for the mouse Wnt cDNAs, G. Walz for the gift of the Myr/Pal Dvl construct, B. Yoder for the gift of anti-polaris/IFT88 antibody and S. Leach for the validated β-catenin antibody. This work was supported by grants from the German Academic Exchange Service (J.G.), the Polycystic Kidney Disease Foundation (J.B.), the National Institute of Child Health and Development (N.K.), the National Institute of Diabetes, Digestive and Kidney disorders (N.K.), the National Institute for Arthritis and Musculoskeletal disorders (S.F.) and the Medical Research Council (P.L.B.). P.L.B. is a Senior Wellcome Trust Fellow. P.A.B. is an Investigator of the Howard Hughes Medical Institute.

Published online at http://www.nature.com/naturegenetics
Reprints and permissions information is available online at http://npg.nature.com/reprintsandpermissions

1. Logan, C.Y. & Nusse, R. The Wnt signaling pathway in development and disease. *Annu. Rev. Cell Dev. Biol.* **20**, 781–810 (2004).
2. Veeman, M.T., Axelrod, J.D. & Moon, R.T. A second canon: functions and mechanisms of beta-catenin-independent Wnt signaling. *Dev. Cell* **5**, 367–377 (2003).
3. Aberle, H., Bauer, A., Stappert, J., Kispert, A. & Kemler, R. beta-catenin is a target for the ubiquitin-proteasome pathway. *EMBO J.* **16**, 3797–3804 (1997).
4. Yan, D. *et al.* Elevated expression of axin2 and hnkd mRNA provides evidence that Wnt/beta-catenin signaling is elevated in human colon tumors. *Proc. Natl. Acad. Sci. USA* **98**, 14973–14978 (2001).
5. Jho, E.H. *et al.* Wnt/beta-catenin/Tcf signaling induces the transcription of Axin2, a negative regulator of the signaling pathway. *Mol. Cell. Biol.* **22**, 1172–1183 (2002).
6. Axelrod, J.D., Miller, J.R., Shulman, J.M., Moon, R.T. & Perrimon, N. Differential recruitment of Dishevelled provides signaling specificity in the planar cell polarity and Wingless signaling pathways. *Genes Dev.* **12**, 2610–2622 (1998).
7. Boutros, M., Paricio, N., Strutt, D.I. & Mlodzik, M. Dishevelled activates JNK and discriminates between JNK pathways in planar polarity and wingless signaling. *Cell* **94**, 109–118 (1998).
8. Keller, R. Shaping the vertebrate body plan by polarized embryonic cell movements. *Science* **298**, 1950–1954 (2002).
9. Torban, E., Kor, C. & Gros, P. Van Gogh-like2 (Strabismus) and its role in planar cell polarity and convergent extension in vertebrates. *Trends Genet.* **20**, 570–577 (2004).
10. Curtin, J.A. *et al.* Mutation of Celsr1 disrupts planar polarity of inner ear hair cells and causes severe neural tube defects in the mouse. *Curr. Biol.* **13**, 1129–1133 (2003).
11. Greene, N.D.E., Gerrelli, D., Van Straaten, H.W.M. & Copp, A.J. Abnormalities of floor plate, notochord and somite differentiation in the loop-tail (Lp) mouse: a model of severe neural tube defects. *Mech. Dev.* **73**, 59–72 (1998).
12. Kibar, Z. *et al.* Ltap, a mammalian homolog of *Drosophila* Strabismus/Van Gogh, is altered in the mouse neural tube mutant loop-tail. *Nat. Genet.* **28**, 251–255 (2001).
13. Kibar, Z. *et al.* Identification of a new chemically induced allele (Lp(m1Jus)) at the loop-tail locus: Morphology, histology, and genetic mapping. *Genomics* **72**, 331–337 (2001).
14. Montcouquiol, M. *et al.* Identification of Vangl2 and Scrb1 as planar polarity genes in mammals. *Nature* **423**, 173–177 (2003).
15. Huangfu, D. *et al.* Hedgehog signalling in the mouse requires intraflagellar transport proteins. *Nature* **426**, 83–87 (2003).
16. Corbit, K.C. *et al.* Vertebrate Smoothened functions at the primary cilium. *Nature* **437**, 1018–1021 (2005).
17. Liu, A.M., Wang, B.L. & Niswander, L.A. Mouse intraflagellar transport proteins regulate both the activator and repressor functions of Gli transcription factors. *Development* **132**, 3103–3111 (2005).
18. Ross, A.J. *et al.* Disruption of Bardet-Biedl syndrome ciliary proteins perturbs planar cell polarity in vertebrates. *Nat. Genet.* **37**, 1135–1140 (2005).
19. Badano, J.L. *et al.* Dissection of epistasis in oligogenic Bardet-Biedl syndrome. *Nature* **439**, 326–330 (2006).
20. Marlow, F., Gonzalez, E.M., Yin, C.Y., Rojo, C. & Solnica-Krezel, L. No tail co-operates with non-canonical Wnt signaling to regulate posterior body morphogenesis in zebrafish. *Development* **131**, 203–216 (2004).
21. Heisenberg, C.P. *et al.* Silberblick/Wnt11 mediates convergent extension movements during zebrafish gastrulation. *Nature* **405**, 76–81 (2000).
22. Ishitani, T. *et al.* The TAK1-NLK-MAPK-related pathway antagonizes signalling between β-catenin and transcription factor TCF. *Nature* **399**, 798–802 (1999).
23. Weidinger, G., Thorpe, C., Wuennenberg-Stapleton, K., Ngai, J. & Moon, R. The Sp1-related transcription factors sp5 and sp5-like act downstream of Wnt/beta-catenin signaling in mesoderm and neuroectoderm patterning. *Curr. Biol.* **15**, 489–500 (2005).
24. Wessely, O., Agius, E., Oelgeschlager, M., Pera, E. & Robertis, E.D. Neural induction in the absence of mesoderm: beta-catenin-dependent expression of secreted BMP antagonists at the blastula stage in *Xenopus*. *Dev. Biol.* **234**, 161–173 (2001).
25. Nojima, H. *et al.* Genetic evidence for involvement of maternally derived Wnt canonical signaling in dorsal determination in zebrafish. *Mech. Dev.* **121**, 371–386 (2004).
26. Rosenbaum, J.L. & Child, F.M. Flagellar regeneration in protozoan flagellates. *J. Cell Biol.* **34**, 345–364 (1967).
27. Veeman, M.T., Slusarski, D.C., Kaykas, A., Louie, S.H. & Moon, R.T. Zebrafish prickle, a modulator of noncanonical Wnt/Fz signaling, regulates gastrulation movements. *Curr. Biol.* **13**, 680–685 (2003).
28. Kim, J.C. *et al.* The Bardet-Biedl protein BBS4 targets cargo to the pericentriolar region and is required for microtubule anchoring and cell cycle progression. *Nat. Genet.* **36**, 462–470 (2004).
29. Korinek, V. *et al.* Constitutive transcriptional activation by a β-catenin–Tcf complex in $APC^{-/-}$ colon carcinoma. *Science* **275**, 1784–1787 (1997).
30. Marszalek, J.R., Ruiz-Lozano, P., Roberts, E., Chien, K.R. & Goldstein, L.S.B. Situs inversus and embryonic ciliary morphogenesis defects in mouse mutants lacking the KIF3A subunit of kinesin-II. *Proc. Natl. Acad. Sci. USA* **96**, 5043–5048 (1999).
31. Sawa, A., Khan, A.A., Hester, L.D. & Snyder, S.H. Glyceraldehyde-3-phosphate dehydrogenase: Nuclear translocation participates in neuronal and nonneuronal cell death. *Proc. Natl. Acad. Sci. USA* **94**, 11669–11674 (1997).
32. Itoh, K., Brott, B.K., Bae, G.-U., Ratcliffe, M.J. & Sokol, S.Y. Nuclear localization is required for Dishevelled function in Wnt/beta-catenin signaling. *J. Biol.* **4**, 1 (2005).
33. Olson, D.J. & Papkoff, J. Regulated expression of Wnt family members during proliferation of C57mg mammary cells. *Cell Growth Differ.* **5**, 197–206 (1994).
34. Shimizu, H. *et al.* Transformation by Wnt family proteins correlates with regulation of beta-catenin. *Cell Growth Differ.* **8**, 1349–1358 (1997).
35. Slusarski, D.C., Corces, V. & Moon, R. Interaction of Wnt and a Frizzled homologue triggers G-protein-linked phosphatidylinositol signalling. *Nature* **390**, 410–413 (1997).
36. Chiang, A.P. *et al.* Homozygosity mapping with SNP arrays identifies TRIM32, an E3 ubiquitin ligase, as a Bardet-Biedl syndrome gene (BBS11). *Proc. Natl. Acad. Sci. USA* **103**, 6287–6292 (2006).
37. Wigley, W.C. *et al.* Dynamic association of proteasomal machinery with the centrosome. *J. Cell Biol.* **145**, 481–490 (1999).
38. DeMartino, G.N. Purification of PA700, the 19S regulatory subunit of the 26S proteasome. *Methods Enzymol.* **398**, 295–306 (2005).

39. Deveraux, Q., Ustrell, V., Pickart, C. & Rechsteiner, M. A 26 S protease subunit that binds ubiquitin conjugates. *J. Biol. Chem.* **269**, 7059–7061 (1994).
40. Deveraux, Q., Jensen, C. & Rechsteiner, M. Molecular cloning and expression of a 26S proteasome subunit enriched in dileucine repeats. *J. Biol. Chem.* **270**, 23726–23729 (1995).
41. Gherman, A., Davis, E. & Katsanis, N. The ciliary proteome database: an integrated community resource for the genetic and functional dissection of cilia. *Nat. Genet.* **38**, 961–962 (2006).
42. Nusse, R. Wnt signaling in disease and in development. *Cell Res.* **15**, 28–32 (2005).
43. Ishitani, T. *et al.* The TAK1-NLK mitogen-activated protein kinase cascade functions in the Wnt-5a/Ca^{2+} pathway to antagonize Wnt/beta-catenin signaling. *Mol. Cell. Biol.* **23**, 131–139 (2003).
44. Liang, H. *et al.* Wnt5a inhibits B cell proliferation and functions as a tumor suppressor in hematopoietic tissue. *Cancer Cell* **4**, 349–360 (2003).
45. Mikels, A.J. & Nusse, R. Purified Wnt5a protein activates or inhibits beta-catenin–TCF signaling depending on receptor context. *PLoS Biol.* **4**, e115 (2006).
46. Topol, L. *et al.* Wnt-5a inhibits the canonical Wnt pathway by promoting GSK-3-independent beta-catenin degradation. *J. Cell Biol.* **162**, 899–908 (2003).
47. Simons, M. *et al.* Inversin, the gene product mutated in nephronophthisis type II, functions as a molecular switch between Wnt signalling pathways. *Nat. Genet.* **37**, 537–543 (2005).
48. Davis, E.E., Brueckner, M. & Katsanis, N. The emerging complexity of the vertebrate cilium: new functional roles for an ancient organelle. *Dev. Cell* **11**, 9–19 (2006).
49. Thisse, C., Thisse, B., Schilling, T.F. & Postlethwait, J.H. Structure of the zebrafish snail1 gene and its expression in wild-type, spadetail and no tail mutant embryos. *Development* **119**, 1203–1215 (1993).
50. Willert, K. *et al.* Wnt proteins are lipid-modified and can act as stem cell growth factors. *Nature* **423**, 448–452 (2003).